Identification of Material Constitutive Laws Representative of Machining Conditions for Two Titanium Alloys: Ti6Al4V and Ti555-3

G. Germain
e-mail: guenael.germain@ensam.eu

A. Morel
e-mail: anne.morel@ensam.eu

Arts et Métiers ParisTech,
LAMPA-EA1427,
2 Bd de Ronceray,
Angers, 49000 France

T. Braham-Bouchnak
IUT Nantes, IRCCyN,
2 avenue du Professeur Jean Rouxel,
Carquefou, 44475 France
e-mail: tarek.braham-bouchnak@univ-nantes.fr

Determining a material constitutive law that is representative of the extreme conditions found in the cutting zone during machining operations is a very challenging problem. In this study, dynamic shear tests, which reproduce, as faithfully as possible, these conditions in terms of strain, strain rate, and temperature, have been developed using hat-shaped specimens. The objective was to identify the parameters of a Johnson–Cook material behavior model by an inverse method for two titanium alloys: Ti6Al4V and Ti555-3. In order to be as representative as possible of the experimental results, the parameters of the Johnson–Cook model were not considered to be constant over the total range of the strain rate and temperature investigated. This reflects a change in the mechanisms governing the deformation. The shear zones observed in hat-shaped specimens were analyzed and compared to those produced in chips during conventional machining for both materials. It is concluded that the observed shear bands can be classified as white-etching bands only for the Ti555-3 alloy. These white bands are assumed to form more easily in the Ti555-3 alloy due to its predominately β phase microstructure compared to the Ti6Al4V alloy with a $\alpha + \beta$ microstructure. [DOI: 10.1115/1.4023674]

1 Introduction

The difficulties associated with the machining of titanium alloys are well known in industry; in the scientific literature these alloys are classed as being "hard to machine" due to their physico-chemical and thermomechanical properties [1–3]. These materials have low thermal conductivity that limits heat transfer and causes high localized temperatures in the cutting zone (>1000 °C). The chips formed in typical cutting conditions are fragmented. The pioneering work of Shaw [4] in the early 1950s attempted to better understand the mechanism of chip formation in titanium alloys. This author suggested that the creation of fragmented chips was linked to instability during cutting that resulted from a competition between thermal softening and strain-hardening mechanisms in the primary shear zone. Later, Komanduri [5] and Barry [6] came to similar conclusions: Komanduri by undertaking orthogonal cutting tests inside a scanning electron microscope and by filming chip formation and Barry by acoustic emission measurements. The chip fragmentation is linked to the temperature increase at the tool tip, which can cause the transformation of a hexagonal close-packed α phase structure, with only a few slip systems, to a body-centered cubic β phase structure, with more slip systems [7,8]. The increased number of slip systems allows for greater strain localization [9]. This, in association with a significant and localized increase in temperature, promotes the formation of adiabatic shear bands [10] enabling the fragmentation of the chip. However, certain authors report that no phase change occurs in the shear bands during the machining process [11]. According to other authors, the formation of saw-tooth shaped chips could also be attributed to the periodic development of cracks from the outer surface of the chip in the primary shear zone [12]. This type of investigation is important even if the study of chip morphology is not an end in itself. It provides information about the cutting process, which can improve the productivity of the machining of titanium alloys by increasing the integrity of the machined surface and the wear behavior of the tool [13]. At the same time, numerical modeling methods have proven effective [14] and the performance of finite element analysis (FEA) software has improved [15]. It is now possible with commercial general purpose FEA software packages [16] to have an overview of the chip formation mechanisms, as quantitative data concerning the transient stress, strain, and temperature fields can be obtained in the cutting zone. These results, however, only have meaning if suitable material models are used. Finding a material behavior model that is representative of the extreme conditions in the cutting zone remains a major challenge that must be overcome. The strain rates in the primary shear zone are estimated to be in the range of 10^4–10^6 s^{-1} in conventional machining [17]. By using the finite element method Shih [18] estimated that the heating and cooling rates can be up to 106 K/s. In addition these loads occur in very localized zones, which results in very high gradients.

The objective of this work is, therefore, to determine the material behavior models representative of the extreme conditions encountered during a machining operation for two titanium alloys: Ti6Al4V and Ti555-3. A Johnson–Cook constitutive model is used and is briefly described in Sec. 2. In order to identify the parameters of the law, specific and adapted mechanical tests have been developed. In particular "hat-shaped" specimens have been used. Section 3 presents the experimental setup and the principal results. Section 4 is devoted to the identification of the parameters of the constitutive model by an inverse method. These parameters are compared to the corresponding coefficients found in the literature for the Ti6Al4V alloy. Special attention is given to the test conditions described in the bibliography. The analysis of the shear zones in chips and hat-shaped specimens is presented in Sec. 5 for both titanium alloys. Section 6 concludes the paper highlighting the main results of the study.

Table 1 Chemical composition (in weight percent) of the two titanium alloys investigated

	Al	V	Cr	Mo	Fe	H	C	O	N	Al eq. value	Mo eq. value
Ti555-3	4.91	5.25	2.98	5.22	0.35	0.001	0.008	0.135	0.006	6.32	18.71
Ti6Al4V	6.02	4.09	-	-	0.06	0.001	0.015	0.16	0.006	7.68	2.92

Al equivalent weight value (%) = Al + Sn/3 + Zr/6 + 10(O +N).
Mo equivalent weight value (%)=Mo + 2 V/3 + Nb/3 + 3 (Fe + Cr).

2 Experimental Investigation

2.1 Materials. The investigations focus on two titanium alloys: Ti555-3 and Ti6Al4V. The chemical composition of these materials is presented in Table 1.

Note that the microstructure of the two materials is very different (Fig. 1). It is due to presence of elements called α (α) stabilizers like Al, O, N… or elements called β (β) stabilizers like Mo, V, Fe, Cr…, which, respectively, promote the formation of α phase and β phase. Considering chemical composition, Table 1 gives the value of aluminum and molybdenum equivalent parameters for both alloys. The Ti6Al4V titanium alloy is a two phase alloy ($\alpha + \beta$) composed of hexagonal close-packed (hcp) α grains and an intergranular β phase (Fig. 1(*b*)). The Ti555-3 alloy consists of a β matrix with a body-centered cubic (bcc) structure and α particles in the form of nodules, ranging in size from about 1 μm to 5 μm (Fig. 1(*a*)). The end of the allotropic phase transformation from α to β phase occurs between 930 °C and 960 °C for the Ti6Al4V alloy and around 845 °C for the Ti555-3 alloy [19].

2.2 Loading Types Encountered in Machining. During machining, three zones of intense deformation determine the chip formation (Fig. 2). The primary zone (ZI) is home to large deformations (several hundred percent), very high strain rates (up to 10^4–10^6 s^{-1}) and a temperature increase estimated to be several hundred degrees Celsius. This zone is subjected to very high shear stresses. The secondary (ZII) and tertiary (ZIII) zones are due to intense friction at the tool-chip interface and the tool–workpiece interface, respectively. These zones are also subject to shear stresses that result in an increase in temperature that can exceed 1000 °C.

Thermomechanical tests are used to identify the material constitutive model, for a given material, to be used for the numerical modeling of machining operations. These tests must be able to reproduce, as faithfully as possible, the extreme shear stress conditions.

2.3 Extreme Shear Tests. The thermomechanical tests undertaken in this work are performed using specimens referred to as hat-shaped specimens, developed by Hartmann [20]. They are typically tested at high strain rates for metallographic analyses. This geometry was tested by Meyers for an α-hcp titanium using a compression Kolsky bar apparatus [21]. It results in the creation of a localized shear zone (Fig. 3) by loading the specimen in compression. Optical micrographs show that the shear zone is cylindrically shaped and located between the cylinder and the bore of the specimen [21]. The degree of localization depends on the difference in diameter between the cylinder and the bore. For the geometry used in this work, the strain rate obtained in the shear zone is ten times greater than the displacement speed at which the specimen is crushed in millimeters per second. For example, for a compression speed of 1 m/s the resulting strain rate is 10^4 s^{-1}.

To achieve these large strain rates, the tests were conducted on a Gleeble thermomechanical simulator. This machine is capable of conducting tests at high temperature (max. 1500 °C) by resistive heating. To improve the electrical contact and to minimize the friction between the specimen and the anvils a nickel-based high temperature lubricant is applied at these interfaces.

The temperature measurements are carried out by two thermocouples welded onto the surface of the specimen as close as possible to the deformation zone. The force is measured by a load cell placed in series with the grips. The movement of the grips can be measured in two different ways depending on the test speed. At low strain rates (less than 10 mm/s) the displacement is measured using a *linear variable differential transformer* (LVDT) attached to the grips. For high test speeds, the hydraulic actuator is decoupled from the movable grip. It is accelerated to the desired speed and impacts the movable grip to achieve high strain rates. In this type of test the LVDT may be damaged. The displacement is then measured by the sensor giving the position of the hydraulic actuator. These displacement measurements, therefore, include the deformation of the grips in addition to the deformation of the specimen. It is, therefore, necessary to correct the force-displacement curves to take into account the stiffness of the experimental setup. In the following, only the corrected force-displacement curves are presented for analysis.

The tests are conducted in a primary vacuum (10^{-2} Torr) for tests at ambient temperature and in a secondary vacuum (10^{-5} Torr) for high temperature tests. In the latter case, the thermomechanical cycle consists of heating the material with a relatively slow heating rate (5 °C/s) to the desired test temperature. This temperature is then maintained for 20 s to ensure that the temperature is uniform within the specimen. The mechanical test is then performed at the desired displacement speed. The repeatability of the result is systematically verified.

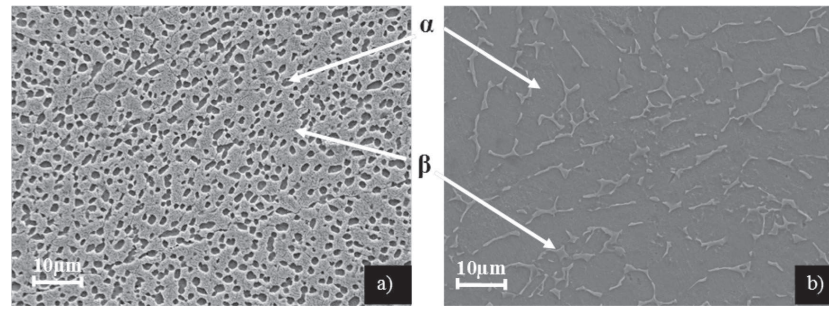

Fig. 1 Microstructures of the two titanium alloys investigated (*a*) Ti555-3 and (*b*) Ti6Al4V

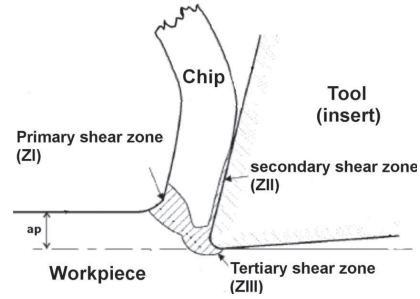

Fig. 2 Shear zones created during the cutting process

The tests are performed on both titanium alloys at temperatures ranging from ambient temperature to 1000 °C and at strain rates ranging from 1 s^{-1} to 10^4 s^{-1}.

2.4 The Influence of the Temperature. Tests at different temperatures are conducted at low strain rates to avoid significant self-heating effects in the shear zone during deformation. For the titanium alloys studied, the force-displacement curves obtained from these tests are shown in Fig. 4.

A drop in axial force can be clearly seen for both alloys when the temperature increases. More specifically, the yield stress decreases with increasing temperature. This can be attributed to an increase in the density of mobile dislocation. Three types of behavior can be seen:

— For low temperatures ($T < 0.3T_f$ or $T < 500$ °C), the force continues to increase with the displacement. Strain-hardening mechanisms seem to dominate.

— For intermediate temperatures (0.3 $T_f < T < 0.5$ T_f or 500 °C $< T <$ 800 °C), after increasing, the force decreases. This behavior has also been observed by other authors [22], who attribute these effects to a competition between the hardening mechanisms and thermal softening effects. Ankem [23] suggests a phenomenon of dynamic recovery. In this domain, the dislocations are annihilated faster than they are created. For the Ti555-3 alloy, the effect of thermal softening occurs earlier than for the Ti6Al4V alloy. The Ti555-3 alloy is richer in the β phase (bcc), which has been proven more sensitive to dynamic recovery compared to the α phase (hcp) [23].

— For high temperatures ($T > 0.5$ T_f or $T > 800$ C), the behavior of two materials is different. For the Ti555-3 alloy the form of the curve changes. Strain hardening becomes once again the dominant phenomenon. For the Ti6Al4V alloy, at 900 °C, the strain hardening mechanism is followed by a series of oscillations with decreasing amplitude before reaching a so-called stationary regime. Via metallurgical observations Ding and Guo noted similar effects for this alloy that they attribute to dynamic recrystallization that occurs during thermomechanical processing in the β phase field [24].

These observations help to understand the metallurgical phenomena that occur during the test.

2.5 Influence of the Strain Rate. Tests with different strain rates are performed at ambient temperature. The force-displacement curves obtained for the two materials are shown in Fig. 5.

It can be seen that there exists two distinct domains in terms of the sensitivity to the strain rate. The first is the quasi-static domain where the strain rate does not seem to have an important influence on the force ($\dot{\bar{\varepsilon}} < 100$ s^{-1}). The second domain corresponds to dynamic tests, for which the force depends more strongly on the strain rate. Figure 6 shows the evolution of the maximum force obtained during the previously discussed tests as a function of the displacement rate. Higher strain rates tend to increase the material's strength due to higher flow stress for both alloys (β Ti555-3 and $\alpha+\beta$ Ti6Al4V).

3 Identification of the Material Behavior Model for the Two Alloys by an Inverse Method

The choice of an appropriate constitutive law is essential for the numerical modeling of the chip formation process. Describing the material behavior requires knowledge of the interactions between strain rate, temperature, and microstructure effects on the high-strain rate mechanical responses of the alloy. A wide variety of material behavior models have been proposed in the literature to account for these effects. The final choice is usually made by selecting a compromise between the ability of the behavior model to describe the relevant phenomena and the ease with which the model parameters can be experimentally identified.

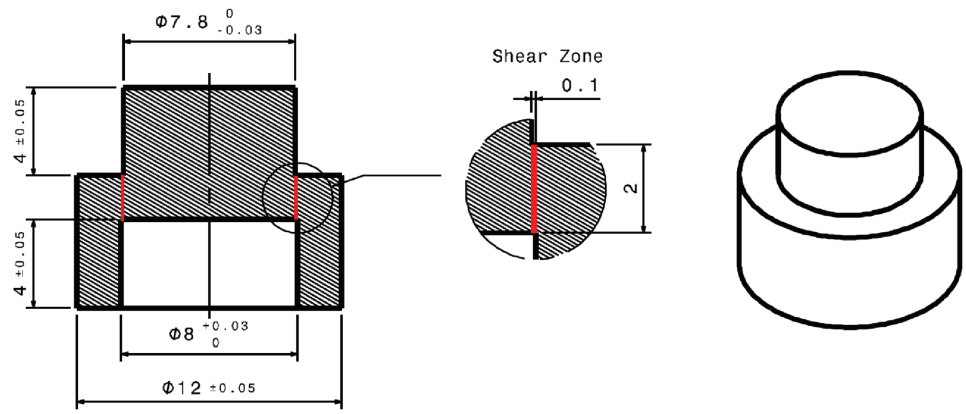

Fig. 3 Hat-shaped specimen

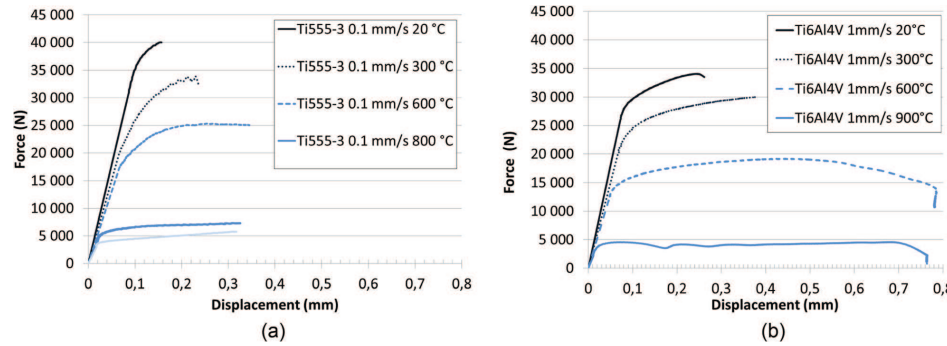

Fig. 4 Force-displacement curves for different temperatures for (*a*) the Ti555-3 alloy and (*b*) the Ti6Al4V alloy

3.1 The Johnson–Cook Material Behavior Model. Johnson and Cook [25] developed a material behavior model to account for the effects of work hardening, the strain rate, and temperature for dynamic loading. It uses a multiplicative formulation that facilitates the identification process. The flow stress is given by the following equation (Eq. (1)):

$$\sigma = \left[A + B\overline{\varepsilon^{p^n}}\right] \cdot \left[1 + C.\mathrm{In}\left(\frac{\dot{\overline{\varepsilon^p}}}{\dot{\overline{\varepsilon^p}}}\right)\right] \cdot \left[1 - \left(\frac{T - T_{\mathrm{ref}}}{T_f - T_{\mathrm{ref}}}\right)^m\right] \quad (1)$$

where σ is the flow stress of the material, $\overline{\varepsilon^p}$ is the equivalent plastic strain, $\dot{\overline{\varepsilon^p}}$ is the equivalent plastic strain rate, T the temperature of the material, T_{ref} the reference temperature, T_f the fusion temperature of the material, $\dot{\overline{\varepsilon_0}}$ the reference equivalent strain rate (here, $\dot{\overline{\varepsilon_0}} = 1$), A is the initial yield stress, B and n are coefficients related to the strain hardening, C is a coefficient controlling the sensitivity to the strain rate, and m controls the sensitivity to the temperature.

This law is the most used for the simulation of machining operations. It is selected for investigation in this work. Other more elaborate models, developed from numerical simulations of chip formation during machining, propose modifications to the Johnson–Cook law to reflect the competition between softening due to the temperature and strain hardening due to the deformation [26,27]. The models of Zerilli and Armstrong [28], on the other hand, are largely inspired by the theory governing the movement of dislocations in the material. They propose an expression for the flow stress as a function of equivalent plastic deformation, the strain rate, temperature, the average diameter of a grain, and the crystallographic structure of the material studied.

3.2 The Identification Procedure. The identification of the Johnson–Cook model requires the estimation of five parameters A, B, C, n and m. The experimental data obtained in the tests described in Sec. 2 with varying temperatures and strain rates are used. The Johnson– Cook law is based on a noncoupled formulation of the terms related to the strain hardening, strain rate, and the temperature. But even if the formulation of the law is noncoupled, the experimental tests are. Indeed, it is not possible to perform a dynamic test at room temperature due to self-heating of the material in the shear zone. This influences the identification process because it is not possible to identify the term controlling the dependence of the strain rate without first identifying the term that controls the temperature dependence.

The general procedure for identifying the parameters of the Johnson–Cook model is as follows:

(1) identification of first three parameters (A, B, n) by quasi-static mechanical tests at room temperature;
(2) identification of the temperature sensitivity parameter (m) by quasi-static tests at different temperatures;
(3) identification of the strain rate sensitivity parameter (C) by testing at different strain rates at an initial ambient temperature.

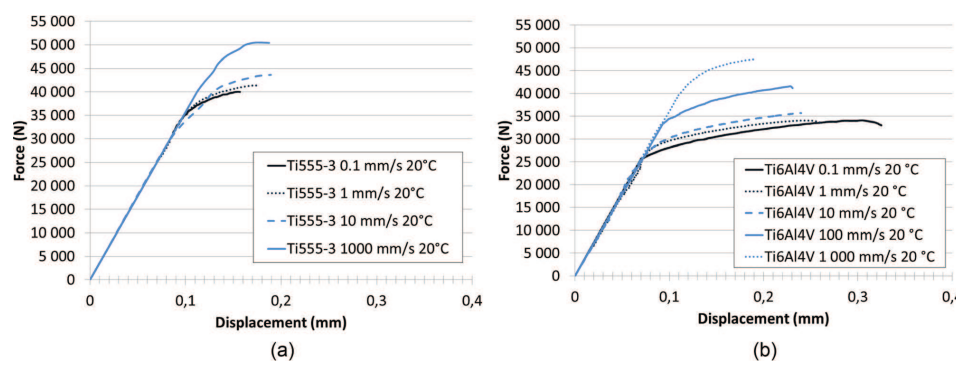

Fig. 5 Force-displacement curves for different displacement rates for (*a*) the Ti555-3 alloy and (*b*) the Ti6Al4V alloy

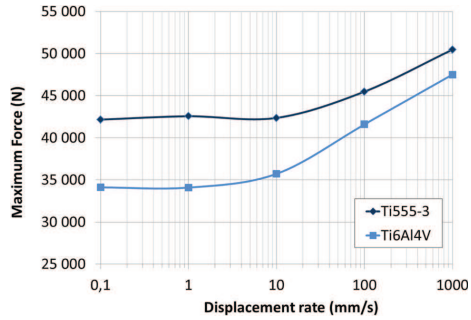

Fig. 6 Evolution of the maximum force as a function of displacement rate

The complexity of the geometry of the hat-shaped specimens does not allow direct calculation of the stress and strain in the shear zone as a function of the force and displacement of the specimen. Numerical modeling must be done in order to identify the parameters of the constitutive model. The commercial finite element code ABAQUS 6.11-1 is used. An explicit integration scheme is used to better taken into account the dynamic aspects of the tests. The specimen is modeled as being a deformable solid and the two grips are modeled as being analytical rigid surfaces. The displacement rate is imposed on the reference point of the mobile grip. The reference point of the fixed grip is completely fixed in order to block all degrees of freedom. The compressive force exerted on the specimen is determined at the reference point of the mobile grip. At this point, it is simple to know at all the times the force and the displacement that can be plotted to establish the numerical force-displacement curve of the test. The specimen is modeled as being 2D axisymmetric. Quadrilateral four-noded elements are used in the shear zone (CAX4RT). The rest of the specimen is meshed with triangular elements (CAX3T) of larger size. The contact interfaces between the specimen and the

Table 2 Starting parameters set for the identification of the two materials

A (MPa)	B (MPa)	C	n	m
968	380	0.0197	0.421	0.577

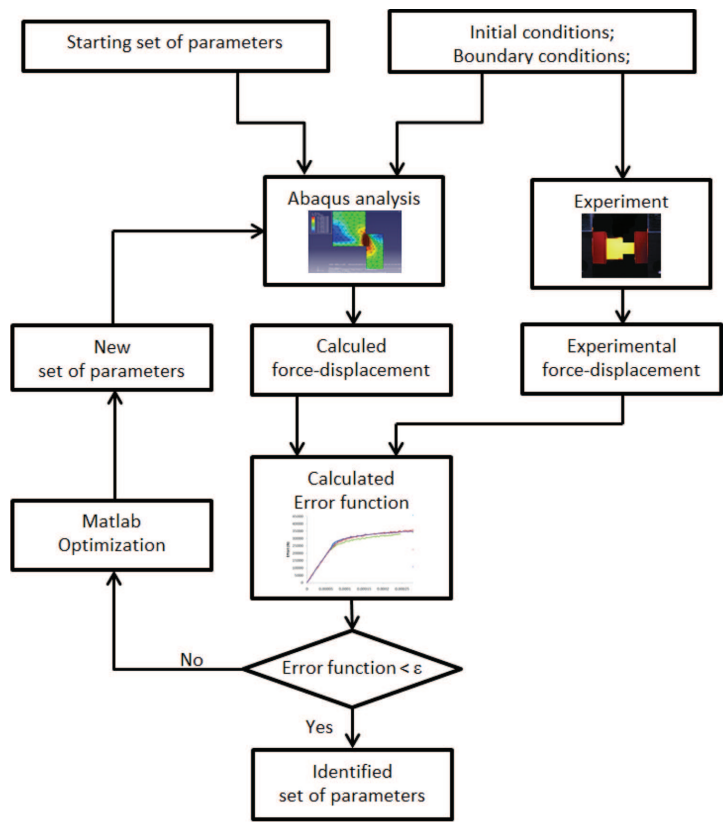

Fig. 7 Flow chart identification procedure of Johnson–Cook parameters

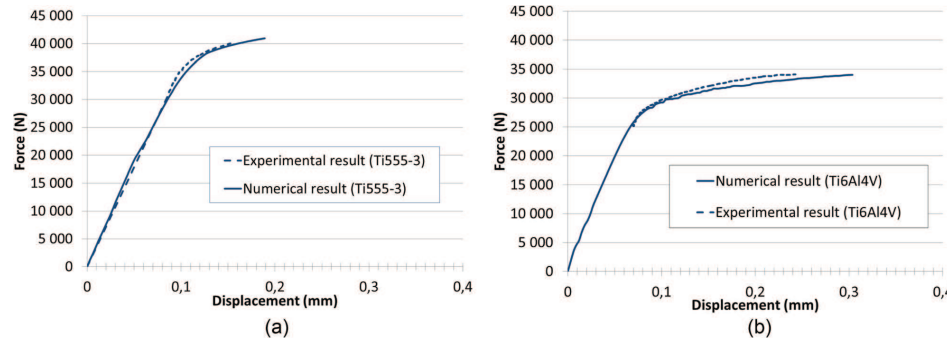

Fig. 8 Experimental and numerical force-displacement curves for (*a*) the Ti555-3 alloy and (*b*) the Ti6Al4V alloy at ambient temperature and quasi-static strain rate

Table 3 Coefficient *A, B, n* identified for the two materials

	A (MPa)	*B* (MPa)	*n*
Ti6Al4V	950	331	0.378
Ti555-3	1175	728	0.260

rigid surfaces representing the grips are assumed to be frictionless. In order to take into account self-heating, the "Self-Heating" coefficient or the Taylor–Quinney empirical constant is set to 0.9. This value is typically used in numerical simulations, which implies that 90% of the plastic deformation energy is converted into thermal energy [29]. To determine the optimum Johnson–Cook parameter set, the Levenberg–Marquardt minimization algorithm [30,31] is used. This algorithm is chosen because of its robustness and fastest convergence. It calculates an error function that compares the experimental force-displacement curves with the numerical curves obtained for a specific Johnson–Cook parameter set. The error function corresponds to the absolute sum of the difference between the two curves for each calculation step. The finite element model is used to compute the force-displacement curve for a given set of fixed parameters. The coefficients of the constitutive model are then modified (i.e., a new parameter set) until the numerical force-displacement curve corresponds to the experimental one. The force-displacement curve is, therefore, the convergence criterion for the identification. The coefficients of the constitutive model are automatically modified by the Levenberg–Marquardt optimization algorithm implemented in Matlab [32]. Figure 7 summarizes the identification procedure.

The starting set of Johnson–Cook parameters is chosen to be the same for both materials studied. These data are the result of the work given in reference Ref. [33] for the Ti6Al4V alloy (see Table 2).

3.3 Identification of the Parameters *A, B,* and *n*. The first step of the identification procedure is to identify the hardening parameters (A, B, and n) using the quasi-static tests at ambient temperature (Fig. 8). The curves obtained, for the best parameter set, show good agreement between the numerical and experimental results.

The resulting best parameter set (A, B, and n) are shown in Table 3 for the two materials

3.4 Identification of the Parameter *m*. The second step is to identify the parameter m by using a series of quasi-static tests at various temperatures. The previously identified hardening parameters are used and m is evaluated for each temperature condition (Fig. 9). The coefficient m is found to be different for each temperature. This indicates that the temperature term in the Johnson–Cook model does not adequately represent the material behavior in terms of temperature over the entire temperature range investigated.

Two temperature zones can be distinguished: one for temperatures below 600 °C and the other at higher temperatures. This

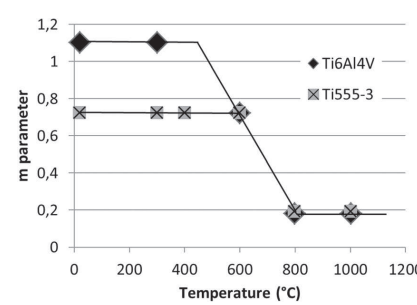

Fig. 9 Evolution of the parameter *m* for the two titanium alloys as a function of temperature

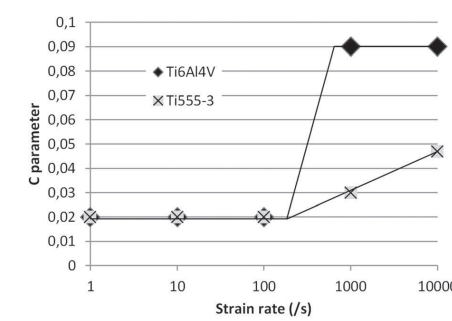

Fig. 10 Evolution of the parameter *C* pour for the two titanium alloys as a function of the strain rate

Table 4 Parameters of the Johnson–Cook model identified for the Ti6Al4V and Ti555-3 titanium alloys

	A (MPa)	B (MPa)	m		C		
			n	$T < 600\,^{\circ}\mathrm{C}$	$T > 600\,^{\circ}\mathrm{C}$	$\dot{\bar{\varepsilon}} < 10^3 S^{-1}$	$\dot{\bar{\varepsilon}} > 10^3 S^{-1}$
Ti6Al4V	950	331	0.378	1.10	0.18	0.020	0.047
Ti555-3	1175	728	0.260	0.72	0.19	0.020	0.090

change in m at approximately 600 °C may correspond to the onset of dynamic recovery [23]. This temperature also fits with the start of the allotropic phase transformation from α to β. During this transformation, the phase ratio is changing with increasing β phase to the detriment of α phase. At higher temperatures, both materials are β phase alloys, which could explain the identical m value.

3.5 Identification of the Parameter *C*. The third step is to identify the parameter C from the results obtained in tests at different strain rates ranging from 1 to 10,000 s^{-1}. Once again, a single value for the parameter C cannot be identified over the entire range of strain rates tested. The results for both alloys are summarized in Fig. 10.

The evolution of the parameter C from a certain strain rate can be related to a change in deformation mechanisms. New slip systems may be activated, particularly in the hcp structure of the Ti6Al4V alloy.

Table 4 summarizes the parameters of the Johnson–Cook model determined in this work for both materials.

3.6 Analysis of the Results. The parameters of the Johnson–Cook model, for the Ti6Al4V alloys, determined from tests performed on split Hopkinson pressure bars (SHPB) were found in the literature. To the authors' knowledge no data are available for the Ti555-3 alloy. Some differences in the parameters found for the Ti6Al4V alloys, particularly in terms of the flow stress data, can be observed in the literature review. The test conditions used for the Ti6Al4V alloy in the literature are listed in Table 5. The results are summarized in Table 6. Note that the parameters obtained from the experimental results of Nemat-Nasser [9] and MacDougall [34] were calculated by Khan [35]. MacDougall is the only author to have carried out shear tests. To exploit their data, Khan [35] converted the shear stress and strain (τ and γ, respectively) to von Mises effective stress and effective plastic strain assuming $\sigma = \tau\sqrt{3}$ and $\varepsilon^p = \gamma\sqrt{3}$ The results obtained from the Gleeble are generally consistent with the bibliographic data; their specificity is to correspond to a large range of strain rates and temperatures and strain levels (evaluated thanks to SEM observations of the deformed grains) that are well above those found in the literature. From the author's point of view, this may explain the differences observed between the results of this study and those found in the literature. The parameter C, in particular, is often identified using a small strain rate range, since the coefficient $\dot{\bar{\varepsilon}}_0$, which acts as a threshold to the strain rate effect, is generally equal to 1 in most studies [9,34–37]. Lee and Lin [22,38] use a lower $\dot{\bar{\varepsilon}}_0$ coefficient, but they identify C for a single strain rate of 2000 s^{-1}. It is, therefore, not surprising to maintain a constant C value. For a larger range of strain rates the mechanisms may change. The value of C can, therefore, evolve. The parameters of the Johnson–Cook model are valid only if the mechanisms remain constant. Other authors have made the same observation [39,40].

Figures 11 and 12 show the comparison between the experimental and numerical curves obtained for the Ti555-3 alloy using

Table 5 Test conditions used for the identification of the Johnson–Cook parameters for the Ti6Al4V alloy

Testing parameters		Largest strain	Strain rate range (s^{-1})	$\dot{\bar{\varepsilon}}(\mathrm{S}^{-1})$	Temperature range (°C)
Lee and Lin [22]	SHPB compression	0.25	2000	10^{-5}	25 1100
Lee and Lin [38]	SHPB compression	0.35	2000	10^{-5}	25 1100
Meyer and Kleponis [36]	SHPB compression	0.57	10^{-4} 10^{-1} 2150	1	20
Lesuer [37]	SHPB compression	0.6	2500 4500	1	20
Nemat-Nasser [9]	SHPB compression	0.6	10^{-3} 1900 2700 3100 3700	1	25 725
Macdougall [34]	SHPB torsion	0.12	4.10^{-4} 0.577 577	1	25
Khan [35]	SHPB compression	0.25	10^{-5} 10^{-3} 1 3378	1	25 482
Present study	Gleeble shear	7 (local value)	1 10 10^2 10^3 10^4 (local values)	1	25 900

Table 6 Comparison between the Johnson–Cook parameters determined for the Ti6Al4V alloy

Reference	A (MPa)	B (MPa)	C		n	m	
Lee and Lin [22]	782.7	498.4	0.028		0.28	1.0	
Lee and Lin [38]	724.7	683.1	0.035		0.47	1.0	
Meyer and Kleponis [36]	862.5	331.2	0.012		0.34	0.8	
Lesuer [37]	1098	1092	0.014		0.93	1.1	
Nemat-Nasser [9]	1119	838.6	0.01921		0.4734	0.6437	
Macdougall [34]	984	520.3	0.015		0.5102	0.8242	
Khan [35]	1080	1007	0.01304		0.5975	0.7701	
Present study	950	331	$\dot{\bar{\varepsilon}} < 10^3 S^{-1}$	$\dot{\bar{\varepsilon}} > 10^3 S^{-1}$	0.378	$T < 600\,°C$	$T > 600\,°C$
			0.020	0.090		1.10	0.18

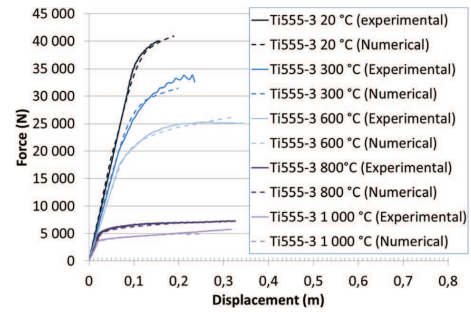

Fig. 11 Comparison between the experimental and numerical force-displacement curves at different temperature for the Johnson–Cook model identified for Ti555-3 alloy (strain rate = 1 s^{-1})

the Johnson–Cook model parameters identified in this study. The good fit validates the obtained coefficients.

4 Analysis of the Shear Zones

After being tested the specimens are sectioned in the axial direction and polished. After etching, they are observed by optical microscope and/or by scanning electron microscope (SEM). For comparison, orthogonal cutting tests are carried out on a lathe on bars of the Ti6Al4V and Ti555-3 titanium alloys with initial diameters of 150 mm and 200 mm in length. The selected tool was a CP500 (Seco) that has a tungsten carbide substrate and a PVD coating of type TiAlN + TiN (rake angle: 5 deg, clearance angle: 7 deg, cutting tool edge radius: 35 μm). The resulting chips are observed under the same conditions as the hat-shaped specimens.

The micrographic observations of chips in the Ti555-3 titanium alloy show the appearance of white bands in the primary and secondary shear zones (Fig. 12). These bands are very hard and resistant to standard etchants used in metallographic studies. These white-etching layers are not observed during machining of the Ti6Al4V alloy, neither in this study nor in those of other authors [10,11,41,42]. They have been observed in the literature for the machining of hard steels [43,44]. The common agreement is that they are composed of very fine grains. The occurrence of a phase transformation is also often discussed. In general, the bands appear after a large rise in temperature and/or intense plastic deformation.

Figure 13 compares the shear zones observed in the Ti6Al4V and Ti555-3 alloys in chips (cutting speed: 60 m/min, feed: 0.2 mm/rev, cutting tool edge radius: 35 μm) and in hat-shaped specimens ($\dot{\varepsilon} = 10^4 s^{-1} - T = 20\,°C$). White bands can be found in the hat-shaped specimen of the Ti555-3 alloy, which are similar to those found in the chips. These observations show that it is possible, in the Ti555-3 alloy, to have the appearance of white bands due to simple dynamic shear with no frictional effects. However, in this study, no white bands are observed in the Ti6Al4V alloy, neither in the hat-shaped specimens nor in the chips.

Other authors have observed this type of white bands in the Ti6Al4V alloy that occur during compression tests on SHPB devices (Table 7). In particular, Xu et al. [45] noticed that during

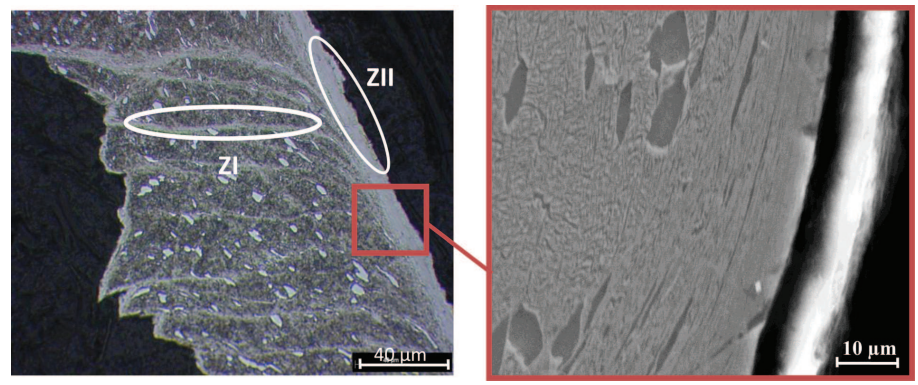

Fig. 12 Observation of white bands in ZI and ZII (Ti555-3, tool CP500, Vc = 90 m/min, f = 0.15 mm/rev)

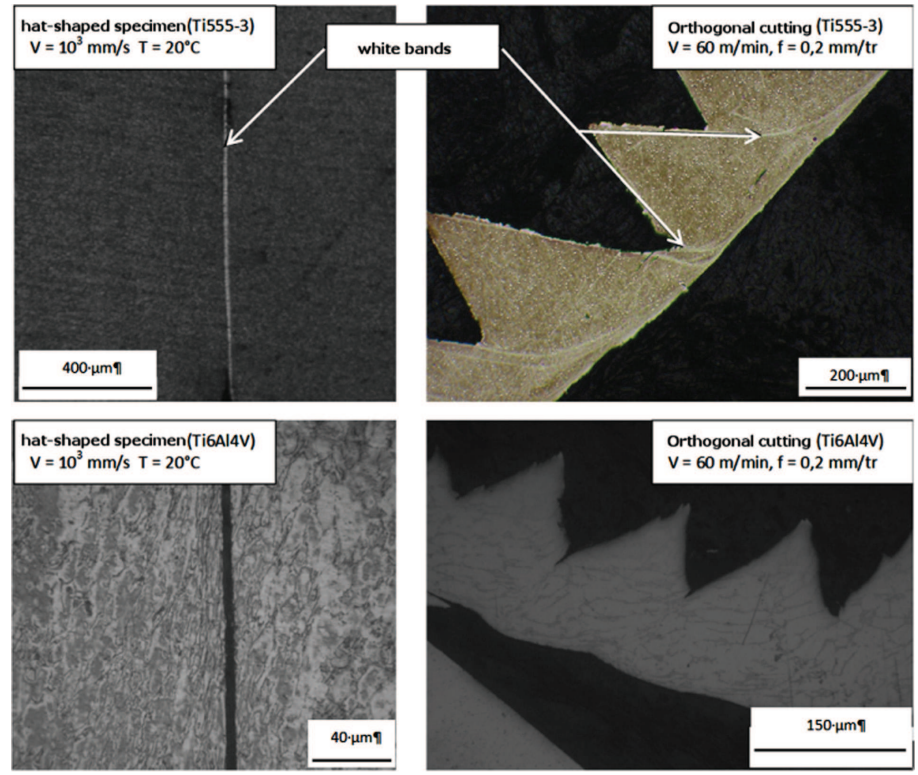

Fig. 13 Comparison between the shear zones created in a hat-shaped specimen and chips formed during machining (Ti555-3)

tests at ambient temperature, the localized shear bands first appear in the form of shear bands deformed up to a strain rate of 1750 s^{-1}. When the strain rate increases the width of the bands decreases. For a strain rate of 2000 s^{-1}, the shear bands are transformed into white-etching bands. It is important to note that in these compression tests under dynamic loading conditions, the plasticity does not spread uniformly in the specimen and is limited to a local region [9,45]. The strain rate measured during compression tests on the SHPB devices is equal to the global strain rate. However, locally the strain rate can be much larger. It is possible that the tests conducted in this study using the Gleeble device do not reach the local strain rates encountered in compression SHPB tests.

Table 7 Summary of the bibliographic data concerning the appearance of white bands in the Ti6AlV4 alloy during SHPB tests

Reference	Temperature (°C)	Strain	Strain rate (s^{-1})	White-etching layers
Nemat-Nasser [9]	725	0.6	3700	Observed
	20	0.35	1900	Observed
	20	0.35	6000	Observed
Lee and Lin [22]	700	0.25	2000	Observed
	1100 °C			
Xu [46]	20	-	2000	Observed
	20	-	1750	Not observed

In the Ti555-3 alloy, the white bands observed in the hat-shaped specimens also appear at low strain rates (1 s^{-1}). Figure 14 shows at this strain rate, the evolution of the thickness of the white bands as a function of test temperature. An increase in temperature seems to favor the formation of white bands.

In order to characterize the white band in the Ti555-3 alloy, a comparison between the phases present in the base material and

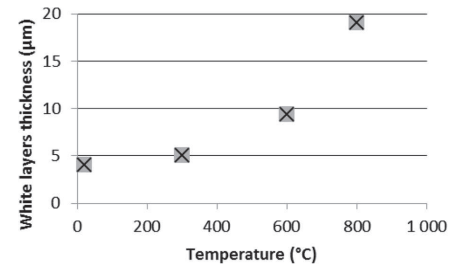

Fig. 14 White band thickness as a function of the test temperature for hat-shaped specimens for the Ti555-3 alloy and a strain rate of 1 s^{-1}

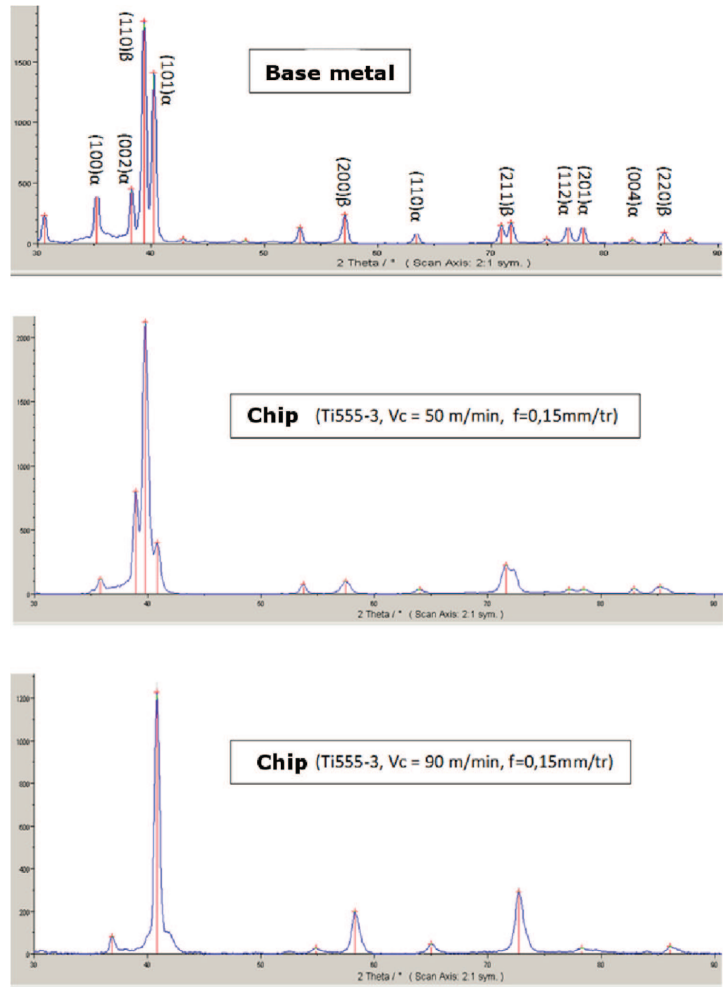

Fig. 15 Phase percentages measured in the base metal and chips resulting from different machining conditions (Ti555-3)

the white bands on the rear face of the chips for different cutting speeds, is carried out (Fig. 15). A diffraction peak analysis shows that the base material is composed of 60.7% β phase and 39.3% α phase. For cutting conditions of $Vc = 50$ m/min and $f = 0.15$ mm/rev, the proportion of α phase in the white bands on the back of the chips decreases sharply to a value of 28.1%. During tests with more severe cutting conditions, ($Vc = 90$ m/min), the white bands have a thickness of approximately 20 μm and are composed of only 11% α phase. Therefore, when the cutting speed increases, the proportion of phase α in the white bands has a tendency to decrease in the Ti555-3 alloy.

These experimental results show that white-etching bands are formed more easily in the Ti555-3 alloy (principally β phase) than in the Ti6Al4V alloy ($\alpha + \beta$ structure). In addition phase transformations from α to β are clearly observed in the formation of white bands. This can probably be partly explained by a lower β-transus temperature in the Ti555-3 alloy than in the Ti6Al4V alloy.

6 Conclusions

From this investigation of the Ti6Al4V and Ti555-3 alloys, it can be concluded that:

(1) Dynamic shear tests were conducted on hat-shaped specimens. These tests are representative of the conditions encountered in machining in terms of strain, strain rate, and temperature and have been used to identify the parameters of the Johnson–Cook material behavior model for two titanium alloys. These results are original for the Ti555-3 alloy.

(2) To be as representative as possible of the experimental results, the parameters of the Johnson–Cook model are not considered to be constant over the range of strain rates and temperatures tested. This reflects a change in the mechanisms governing the deformation.
(3) Microstructural observations of hat-shaped specimens and chips highlight the appearance of shear bands in both materials. The observed bands can be classified as white-etching bands only for the Ti555-3 alloy. The white bands are formed more easily in this alloy due to its predominately β phase structure compared to the Ti6Al4V alloy with a $\alpha + \beta$ structure.
(4) The thickness of the white bands formed in the Ti555-3 alloy increases as the temperature increases.
(5) The proportion of α phase in white bands formed in the Ti555-3 alloy decreases when the cutting conditions become more severe.

References

[1] Ezugwu, E. O., Bonney, J., and Yamane, Y., 2003, "An Overview of the Machinability of Aeroengine Alloys," J. Mater. Process. Tech., **134**(2), pp. 233–253.
[2] Ezugwu, E. O., and Wang, Z. M., 1997, "Titanium Alloys and Their Machinability—A Review," J. Mater. Process. Tech., **68**(3), pp. 262–274.
[3] Ohkubo, C., Watanabe, I., and Ford, J. P., 2000, "The Machinability of Cast Titanium and Ti–6Al–4V," Biomaterials, **21**(4), pp. 421–428.
[4] Shaw, M. C., Dirke, S. O., and Smith, P. A., 1954, "Machining Titanium," MIT Rep., 4th ed., Massachusetts Institute of Technology, Cambridge, MA.
[5] Komanduri, R., and Von Turkovich, B. F., 1981, "New Observations on the Mechanism of Chip Formation When Machining Titanium Alloys," Wear, **69**(2), pp. 179–188.
[6] Barry, J., Byrne, G., and Lennon, D., 2001, "Observations on Chip Formation and Acoustic Emission in Machining Ti-6Al-4V Alloy," Int. J. Mach. Tool. Manu., **41**(7), pp. 1055–1070.
[7] Bayoumi, A. E., and Xie, J. Q., 1995, "Some Metallurgical Aspects of Chip Formation in Cutting Ti-6wt.%Al-4wt.%V Alloy," Mater. Sci. Eng. A, **190**(1–2), pp. 173–180.
[8] Komanduri, R., 1982, "Some Clarifications on the Mechanics of Chip Formation When Machining Titanium Alloys," Wear, **76**(1), pp. 15–34.
[9] Nemat-Nasser, S., Guo, W., and Nesterenko, V. F., 2001, "Dynamic Response of Conventional and Hot Isostatically Pressed Ti-6Al-4V Alloys: Experiments and Modeling," Mech. Mater., **33**(8), pp. 425–439.
[10] Molinari, A., Musquar, C., and Sutter, G., 2002, "Adiabatic Shear Banding in High Speed Machining of Ti-6Al-4V: Experiments and Modeling," Int. J. Plasticity, **18**(4), pp. 443–459.
[11] Puerta Velásquez, J. D., Bolle, B., and Chevrier, P., 2007, "Metallurgical Study on Chips Obtained by High Speed Machining of a Ti–6 wt.%Al–4 wt.%V Alloy," Mater. Sci. Eng. A, **452–453**, pp. 469–474.
[12] Vyas, A., and Shaw, M. C., 1999, "Mechanics of Saw-Tooth Chip Formation in Metal Cutting," ASME J. Manuf. Sci. Eng., **121**(2), pp. 163–172.
[13] Mabrouki, T., and Rigal, J., 2006, "A Contribution to a Qualitative Understanding of Thermo-Mechanical Effects During Chip Formation in Hard Turning," J. Mater. Process. Tech., **176**(1–3), pp. 214–221.
[14] Vaz, Jr., M., Owen, D. R. J., and Kalhori, V., 2007, "Modelling and Simulation of Machining Processes," Arch. Comput. Method. Eng., **14**(2), pp. 173–204.
[15] Guo, Y. B., and Yen, D. W., 2004, "A FEM Study on Mechanisms of Discontinuous Chip Formation in Hard Machining," J. Mater. Process. Tech., **155–156**, pp. 1350–1356.
[16] Dassault Systèmes Simulia, C., 2008, ABAQUS Version 6.8 documentation.
[17] Shrot, A., and Bäker, M., 2012, "Determination of Johnson–Cook Parameters From Machining Simulations," Comp. Mater. Sci., **52**(1), pp. 298–304.
[18] Albert J. S., 1996, "Finite Element Analysis of Orthogonal Metal Cutting Mechanics," Int. J. Mach. Tool. Manu., **36**(2), pp. 255–273.
[19] Hayes, F. H., 1995, "The Al-Ti-V (Aluminum-Titanium-Vanadium) System," J. Phase Equilib., **16**(2), pp. 163–176.
[20] Hartman, K. H., Kunze, H. D., and Meyer, L. W., 1981, "Metallurgical Effects on Impact Loaded Materials," *Shock Waves and High-Strain-Rate Phenomena in Metals*, M. A. Meyers and L. E. Murr, eds., Plenum Press, New York, pp. 325–337.
[21] Meyers, M. A., Subhash, G., and Kad, B. K., 1994, "Evolution of Microstructure and Shear-Band Formation in α-Hcp Titanium," Mech. Mater., **17**(2–3), pp. 175–193.
[22] Lee, W., and Lin, C., 1998, "High-Temperature Deformation Behaviour of Ti6Al4V Alloy Evaluated by High Strain-Rate Compression Tests," J. Mater. Process. Tech., **75**(1–3), pp. 127–136.
[23] Ankem, S., Shyue, J. G., and Vijayshankar, M. N., 1989, "The Effect of Volume Per Cent of Phase on the High Temperature Tensile Deformation of Two-Phase Ti-Mn Alloys," Mater. Sci. Eng. A, **111**, pp. 51–61.
[24] Ding, R., and Guo, Z. X., 2004, "Microstructural Evolution of a Ti-6Al-4V Alloy During β-Phase Processing: Experimental and Simulative Investigations," Mater. Sci. Eng. A, **365**(1–2), pp. 172–179.
[25] Johnson, G. R., and Cook, W. H., 1983, "A Constitutive Model and Data for Metals Subjected to Large Strains, High Strain Rates and High Temperatures," Proceeding 7th International Symposium on Ballistics, The Hague, April 19–21, pp. 541–547.
[26] Bäker, M., 2006, "Finite Element Simulation of High-Speed Cutting Forces," J. Mater. Process. Tech., **176**(1–3), pp. 117–126.
[27] Calamaz, M., Coupard, D., and Girot, F., 2010, "Numerical Simulation of Titanium Alloy Dry Machining With a Strain Softening Constitutive Law," Mach. Sci. Tech., **14**(2), pp. 244–257.
[28] Zerilli, F. J., and Armstrong, R. W., 1987, "Dislocation-Mechanics-Based Constitutive Relations for Material Dynamics Calculations," J. Appl. Phys., **61**(5), pp. 1816–1825.
[29] Lemaitre, J., and Chaboche, J. L., 1990, Mechanics of Solid Materials, Cambridge University Press, Cambridge, MA.
[30] Levenberg, K., 1944, "A Method for the Solution of Certain Nonlinear Problems in Least Squares," Quart. Appl. Math., **2**(2), pp. 164–168.
[31] Marquardt, D. W., 1963, "An Algorithm for Least-Squares Estimation of Nonlinear Parameters," J. Soc. Ind. Appl. Math., **11**(2), pp. 431–441.
[32] Galassi, M., Davies, J., and Theiler, J., 2003, GNU Scientific Library Reference Manual, Network Theory Limited, Bristol, UK.
[33] Cao, Z., He, N., and Li, L., 2008, "Chip Formation and Its Numerical Simulation in High Speed Cutting of Ti6Al4V Alloy," Zhongguo Jixie Gongcheng/Chin. Mech. Eng., **19**(20), pp. 2450–2454.
[34] Macdougall, D. A. S., and Harding, J., 1998, "The Measurement of Specimen Surface Temperature in High-Speed Tension and Torsion Tests," Int. J. Impact Eng., **21**(6), pp. 473–488.
[35] Khan, A. S., Sung Suh, Y., and Kazmi, R., 2004, "Quasi-Static and Dynamic Loading Responses and Constitutive Modeling of Titanium Alloys," Int. J. Plasticity, **20**(12), pp. 2233–2248.
[36] Meyer, Jr., H. W., and Kleponis, D. S., 2001, "Modeling the High Strain Rate Behavior of Titanium Undergoing Ballistic Impact and Penetration," Int. J. Impact Eng., **26**(1–10), pp. 509–521.
[37] Lesuer, D. R., 2000, "Experimental Investigations of Material Models for Ti-6Al-4V Titanium and 2024-T3 Aluminum," Office of Aviation Research (USA), Technical Report PB2001-101864 DOT/FAA/AR-00/25.
[38] Lee, W., and Lin, C., 1998, "Plastic Deformation and Fracture Behaviour of Ti-6Al-4V Alloy Loaded With High Strain Rate Under Various Temperatures," Mater. Sci. Eng. A, **241**(1–2), pp. 48–59.
[39] Hor, A., 2010, "Simulation Physique Des Procédés De Fabrication: Caractérisation De La Rhéologie Et De l'Endommagement Lors d'Opérations De Forgeage Et d'Usinage," Ph.D. thesis, Arts et Métiers ParisTech, France.
[40] Zemzemi, F., 2007, "Caractérisation De Modèles De Frottement Aux Interfaces Pièce-Outil-Copeau En Usinage: Application Au Cas De l'Usinage Des Aciers Et De l'Inconel 718," Ph.D. Thesis, Ecole Centrale de Lyon, France.
[41] Calamaz, M., Coupard, D., and Nouari, M., 2011, "Numerical Analysis of Chip Formation and Shear Localisation Processes in Machining the Ti-6Al-4V Titanium Alloy," Int. J. Adv. Manu. Tech., **52**(9–12), pp. 887–895.
[42] Sun, S., Brandt, M., and Dargusch, M. S., 2009, "Characteristics of Cutting Forces and Chip Formation in Machining of Titanium Alloys," Int. J. Mach. Tool. Manu., **49**(7–8), pp. 561–568.
[43] Ramesh, A., Melkote, S. N., and Allard, L. F., 2005, "Analysis of White Layers Formed in Hard Turning of AISI 52100 Steel," Mater. Sci. Eng. A, **390**(1–2), pp. 88–97.
[44] Poulachon, G., Albert, A., and Schluraff, M., 2005, "An Experimental Investigation of Work Material Microstructure Effects on White Layer Formation in PCBN Hard Turning," Int. J. Mach. Tool. Manu., **45**(2), pp. 211–218.
[45] Xu, Y., Zhang, J., and Bai, Y., 2008, "Shear Localization in Dynamic Deformation: Microstructural Evolution," Metall. Mater. Trans. A, **39**(4), pp. 811–843.
[46] Xu, Y. B., Liu, L., and Yu, J. Q., 2000, "Thermoplastic Shear Localisation in Titanium Alloys During Dynamic Deformation," Mater. Sci. Tech., **16**(6), pp. 609–611.